

Thermal expansion and impurity effects on lattice thermal conductivity of solid argon

Yunfei Chen^{a)}

Department of Mechanical Engineering and China Education Council Key Laboratory of MEMS, Southeast University, Nanjing 210096, People's Republic of China

Jennifer R. Lukes

Department of Mechanical Engineering and Applied Mechanics, University of Pennsylvania, Philadelphia, Pennsylvania 19104-6315

Deyu Li

Department of Mechanical Engineering, University of California, Berkeley, California 94720-1740

Juekuan Yang and Yonghua Wu

Department of Mechanical Engineering and China Education Council Key Laboratory of MEMS, Southeast University, Nanjing 210096, People's Republic of China

(Received 13 October 2003; accepted 1 December 2003)

Thermal expansion and impurity effects on the lattice thermal conductivity of solid argon have been investigated with equilibrium molecular dynamics simulation. Thermal conductivity is simulated over the temperature range of 20–80 K. Thermal expansion effects, which strongly reduce thermal conductivity, are incorporated into the simulations using experimentally measured lattice constants of solid argon at different temperatures. It is found that the experimentally measured deviations from a T^{-1} high-temperature dependence in thermal conductivity can be quantitatively attributed to thermal expansion effects. Phonon scattering on defects also contributes to the deviations. Comparison of simulation results on argon lattices with vacancy and impurity defects to those predicted from the theoretical models of Klemens and Ashegi *et al.* demonstrates that phonon scattering on impurities due to lattice strain is stronger than that due to differences in mass between the defect and the surrounding matrix. In addition, the results indicate the utility of molecular dynamics simulation for determining parameters in theoretical impurity scattering models under a wide range of conditions. It is also confirmed from the simulation results that thermal conductivity is not sensitive to the impurity concentration at high temperatures. © 2004 American Institute of Physics. [DOI: 10.1063/1.1643725]

I. INTRODUCTION

The thermal conductivity of a dielectric material depends on temperature, sample size, and defect concentration. At very low temperatures phonon transport is dominated by boundary scattering, leading to size-dependent thermal conductivity. As temperature increases, thermal conductivity first increases due to increasing population of higher phonon energy levels, and reaches a peak value, which is determined by impurity concentration, and then decreases due to impurity scattering. At still higher temperatures, three-phonon Umklapp scattering processes begin to become important, and combine with impurity scattering effects to reduce further the thermal conductivity.¹ Above the Debye temperature the lifetime of three-phonon scattering processes is inversely proportional to temperature while the specific heat and phonon group velocity are temperature independent. In combination with the kinetic theory of phonon gases, this leads to the well-known T^{-1} behavior of the thermal conductivity of dielectric materials. In practice the T^{-1} behavior is actually

observed at some fraction of the Debye temperature, for example at 1/4 of the Debye temperature for argon and at 1/10 of the Debye temperature for silicon.

Experimental work by Krupskii and Manzhelli on unconstrained argon samples² revealed a quadratic temperature term in addition to the theoretically predicted inverse temperature dependence. They attributed this extra term to higher-order four-phonon interactions while Clayton and Batchelder³ attributed it to thermal expansion effects. Dugdale and MacDonald⁴ postulated that the differential lattice expansion in the presence of a temperature gradient, for example, the relative expansion of hotter regions and compression of cooler regions for materials with a positive thermal expansion coefficient, creates another source of momentum transfer that further reduces thermal conductivity beyond that determined by three-phonon processes alone. Using the kinetic theory of phonon gases, they linked thermal conductivity to thermal expansion by defining the phonon mean free path as the inverse product of thermal expansion coefficient and temperature. Christen and Pollack,⁵ whose experimental work agrees well with first principle calculations on the contribution of the anharmonic crystal force to thermal resistance, also attributed the deviation from T^{-1} behavior to the

^{a)}Electronic mail: yunfeichen@yahoo.com

effects of thermal expansion on the lattice vibrational frequencies.

Several experimental and theoretical investigations have also been performed to study the effects of isotopes, impurities, and defects on the thermal conductivity.^{6–14} Stachowiak *et al.*¹³ measured the thermal conductivity of solid argon with oxygen impurity in the temperature range of 1.3–26 K and argued that the interaction of phonons with the spin-rotational motion of oxygen molecules provides significant resistance to the phonon transport. Plekhanov¹⁴ showed that 1% ¹³C in natural diamond could lead to a 30% reduction of the room temperature thermal conductivity as compared to isotopically pure diamond. Capinski *et al.*⁸ measured isotopically pure silicon made from 99.7% ²⁸Si by liquid phase epitaxy, and found its thermal conductivity to be over 250% higher at 100 K than that of natural silicon. Asen-Palmer *et al.*⁹ measured a maximum thermal conductivity of 10.5 kW/m K for highly enriched 99.99% ⁷⁰Ge, which is one order of magnitude higher than that of natural germanium.

The dramatic change in thermal conductivity caused by the addition and removal of point lattice imperfections and the disagreement in thermal conductivity temperature dependence between theoretical models and experimental results prompt us to model the effects of thermal expansion and impurities on lattice thermal conductivity. Molecular dynamics simulation is a convenient tool for such a modeling work since it allows precise specification of impurity concentration, lattice parameter, and temperature. Several groups have reported molecular dynamics simulations of thermal conduction and thermal expansion in crystalline materials in recent years. For example, Kaburaki *et al.*¹⁵ performed equilibrium molecular dynamics (EMD) simulations of bulk argon and found the predicted results to be uniformly low, although the calculated temperature dependence was found to correspond well with experimental data. Volz *et al.*¹⁶ used molecular dynamics to test the validity of the Fourier law. Lukes *et al.*¹⁷ predicted the thin film thermal conductivity of solid argon based on nonequilibrium molecular dynamics. Porter *et al.*¹⁸ calculated the thermal expansion coefficient of crystalline silicon carbide. Despite these studies, there has been little research investigating how thermal expansion affects thermal conductivity. The influence of defects on high-temperature thermal conductivity and the potential of molecular dynamics simulation for better understanding the parameters in theoretical models of impurity scattering also remain to be explored. To address these issues, this article examines thermal expansion and impurity effects on thermal conductivity using EMD simulations. The simulations are performed on crystalline argon, one of the best experimentally characterized noble elements.

II. MATHEMATICAL MODEL

The Lennard-Jones 6–12 potential (LJ):

$$V(r) = 4e \left[\left(\frac{\sigma}{r} \right)^{12} - \left(\frac{\sigma}{r} \right)^6 \right] \quad (1)$$

is employed in the present EMD simulations. Here e and σ represent the energy and length scales of the potential, and r

denotes the distance between two particles. Following the Green–Kubo formalism in linear response theory, the lattice thermal conductivity of bulk solid argon is calculated by integrating the heat current correlation function:

$$K = \frac{1}{3Vk_B T^2} \int_0^\infty \langle J(t)J(0) \rangle dt, \quad (2)$$

where T , k_B , and V are absolute temperature, Boltzmann's constant and system volume, respectively. The heat current J is

$$J = \frac{1}{V} \left[\sum_i e_i \mathbf{v}_i + \frac{1}{2} \sum_{i \neq j} \mathbf{r}_{ij} (\mathbf{f}_{ij} \cdot \mathbf{v}_i) \right], \quad (3)$$

where \mathbf{v} is the particle velocity and \mathbf{f}_{ij} is the force acting on the particle i from the particle j . The energy of particle i , e_i , is defined as

$$e_i = \frac{1}{2} m v_i^2 + \frac{1}{2} \sum_i V(r_{ij}). \quad (4)$$

In order to investigate the effects of impurities on the thermal conductivity of solid argon, the semiclassical equation of Callaway⁶ is employed to fit, over a range of temperatures, both existing experimental thermal conductivity measurements and simulation data generated in this article. In this equation,

$$k = \frac{k_B}{2\pi^2 v_s} (I_1 + \beta I_2), \quad (5)$$

v_s is the speed of sound of solid argon and I_1 , I_2 , and β are defined as

$$I_1 = \int_0^{\omega_D} \frac{\tau_c}{\tau_c} \frac{\hbar^2 \omega^2}{k_B^2 T^2} \frac{e^{\hbar\omega/k_B T}}{(e^{\hbar\omega/k_B T} - 1)^2} \omega^2 d\omega, \quad (6)$$

$$I_2 = \int_0^{\omega_D} \frac{\tau_c}{\tau_N} \frac{\hbar^2 \omega^2}{k_B^2 T^2} \frac{e^{\hbar\omega/k_B T}}{(e^{\hbar\omega/k_B T} - 1)^2} \omega^2 d\omega, \quad (7)$$

$$\beta = \int_0^{\theta/T} \frac{\tau_c}{\tau_N} \frac{x^4 e^x}{(e^x - 1)^2} dx \Bigg/ \int_0^{\theta/T} \frac{1}{\tau_N} \left(1 - \frac{\tau_c}{\tau_N} \right) \frac{x^4 e^x}{(e^x - 1)^2} dx, \quad (8)$$

where ω is phonon frequency, ω_D is the Debye cutoff frequency, h is Planck's constant, θ is the Debye temperature:

$$\hbar = h/2\pi, \quad (9)$$

$$x = \hbar\omega/k_B T, \quad (10)$$

$$\theta = \hbar\omega_D/k_B, \quad (11)$$

and τ_c is the combined phonon relaxation time. This relaxation time is comprised of terms accounting for normal (N) and Umklapp (U) three-phonon scattering, boundary scattering, and impurity scattering processes:

$$\tau_c^{-1} = \tau_N^{-1} + \tau_U^{-1} + \tau_b^{-1} + \tau_i^{-1}. \quad (12)$$

For argon, the inverse lifetimes of N and U processes are defined as that in Ref. 19:

$$\tau_N^{-1} + \tau_U^{-1} = (B_1 + B_2)\omega^2 T^3. \tag{13}$$

The relaxation time due to the boundary scattering depends on the phonon group velocity and the characteristic sample dimension l . For single crystals this dimension corresponds to the physical size of the sample, while for polycrystalline materials this dimension corresponds to the grain size. Approximating group velocity as the speed of sound leads to

$$\tau_b^{-1} = v_s/l. \tag{14}$$

Impurity scattering contributes greatly to thermal resistance at low temperatures. The time scale for scattering by impurities is expressed using a simple model by Klemens:¹⁰

$$\tau_i^{-1} = \frac{V_0}{4\pi^2 v_s^3} \sum_{i=1}^n f_i \left(1 - \frac{M_i}{M}\right)^2 \omega^4 = A_i \omega^4, \tag{15}$$

where V_0 is the atomic volume, M_i is the mass of an atom, M is the average mass of all atoms, including impurities, and f_i the fraction of atoms with mass M_i . A_i in Eq. (15) is read as

$$A_i = \frac{V_0}{4\pi^2 v_s^3} \sum_{i=1}^n f_i \left(1 - \frac{M_i}{M}\right)^2. \tag{16}$$

In order to evaluate the theoretical model parameters $B_1 + B_2$ in Eq. (13), l in Eq. (14), and A_i in Eq. (15), the fitting procedure is performed in different temperature regimes. Depending on the regime, least-squares fits are made to either existing experimental data or the present EMD simulations. For the simulations, Callaway's theoretical thermal conductivities calculated from Eq. (5) are fitted to the EMD thermal conductivities calculated using Eq. (2) by adjusting the above parameters. At high temperatures N and U processes dominate and boundary and impurity scattering processes contribute little to the thermal resistance. The sum $B_1 + B_2$ can thus be deduced from the simulation data for pure argon by neglecting the boundary and impurity scattering terms in Eq. (12). At very low temperatures it is inappropriate to fit the Callaway model to the simulation results, as the classical EMD simulations do not correctly predict the quantum effects on thermal conductivity behavior in this regime. Boundary scattering dominates at low temperatures, so the parameter l for boundary scattering is thus determined by neglecting all terms but τ_b^{-1} in Eq. (12) and subsequently fitting the Callaway model to experimental low temperature data on solid argon.⁵ Once the parameters $B_1 + B_2$ and l are evaluated, they can be used to determine the impurity scattering parameter A_i . This is done by fitting Eq. (5) to simulation data in the temperature range between 30 and 60 K where peak thermal conductivity occurs.

III. SIMULATION RESULTS AND DISCUSSION

Simulations are performed in the microcanonical ensemble on face centered cubic solid argon. A cubic simulation box of side L is used, with the usual periodic boundary conditions imposed along the x , y , and z directions. Key simulation parameters are shown in Table I. Different lattice constants were used in the simulations depending on the par-

TABLE I. Simulation parameters.

Variable	Value	Variable	Value
Energy scale of argon in LJ potential ϵ_1 (J)	1.67E-21	Length scale of argon in LJ potential σ_1 (m)	3.4E-10
Energy scale of krypton in LJ potential ϵ_2 (J)	2.25E-21	Length scale of argon in LJ potential σ_2 (m)	3.65E-10
Energy scale for the interactions between Ar and Kr atoms in LJ potential ϵ_{12} (J)	$\sqrt{\epsilon_1 \epsilon_2}$	Length scale for the interactions between Ar and Kr atoms in LJ potential σ_{12} (m)	$(\sigma_1 + \sigma_2)/2$
Atom radius of argon (m)	8.8E-11	Atom radius of krypton (m)	10.3E-11
Atom mass of argon m (kg)	6.63E-26	Atom mass of krypton m_1 (kg)	1.39E-25
Q_0 for vacancy defect	3.2	Q_0 for krypton impurity	4
Lattice constant of argon at 0 K a (m)	5.3E-10	Averaged γ (Ref. 23)	2.5
A_i for vacancy defect (0.39%)	5.56E-41	A_i for krypton impurity (0.39%)	6.09E-41
A_s for vacancy defect (0.39%)	2.84E-38	A_s for krypton impurity (0.39%)	0.25E-38

ticular case of interest and the temperature. The temperature-dependent lattice constants for solid argon of Peterson²⁰ are used.

The final simulation results are found to be very sensitive to the total time steps due to the slow convergence of the Green–Kubo integration. To obtain reliable results by direct integration a very large number of time steps must be used for accurate statistical averaging. In addition, the number of integration steps must be chosen so that the integration time is larger than the characteristic time required for the current–current autocorrelation function to decay to zero. In this article, the total number of time steps is five million. This corresponds to about 5 ns for the heat flux autocorrelation integration. Standard error analysis of the simulation data generated from several runs results in errors in effective thermal conductivity between 10% and 15% of the calculated values in most cases. Below 30 K, cases with high impurity concentrations have an error of 20%, the maximum observed in all simulations.

Figure 1 shows the simulated thermal conductivity in the temperature range of 10–70 K. For all simulations in this

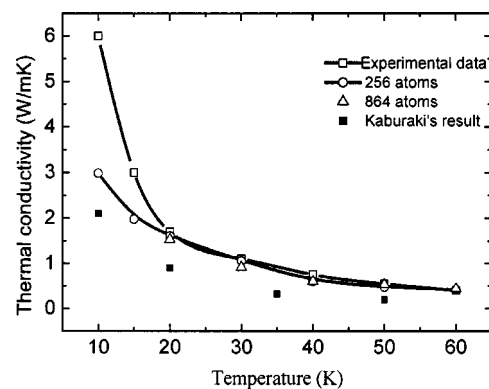


FIG. 1. Thermal conductivity of solid argon-fixed lattice constant.

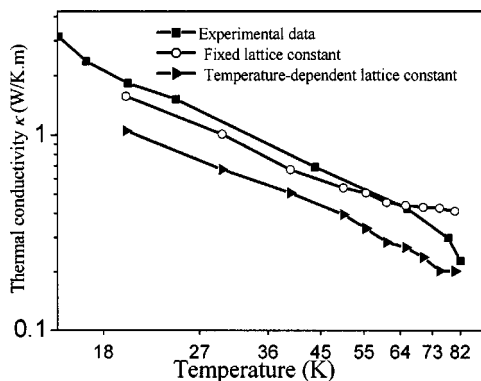


FIG. 2. Thermal expansion effects on thermal conductivity of solid argon.

figure, the lattice constant has been fixed to its 0 K value of 0.53 nm over the entire temperature range. Thermal expansion is thus not taken into account in Fig. 1. The current simulation results lie nearer to the experimental data⁵ than do the previous results of Ref. 15. In contrast to simulations of silicon,²¹ no clear evidence of finite size effects on thermal conductivity is found. Simulations on 256 and 864 atom systems display little dependence on the number of particles in the simulation domain. At temperatures below 20 K, the simulation results diverge from the experimental data. This occurs because the classical EMD simulations do not account for the different quantum occupation of phonon states from the classical Boltzmann distribution that becomes important at temperatures far below the Debye temperature (92 K for argon). Based on these results, EMD can be used to explore thermal expansion effects on lattice thermal conductivity only at temperatures above 20 K.

Along with the experimental data and 864 atom fixed lattice constant data from Fig. 1, Fig. 2 shows thermal expansion effects on lattice thermal conductivity. In these simulations the lattice constant has been varied depending on the temperature. When the temperature exceeds 55 K, the fixed parameter case exhibits a decay of thermal conductivity with increasing temperature that is slow compared to experimental results. The calculations that account for temperature dependence of the lattice parameter show much better agreement with experimental trends. The temperature dependence of the thermal conductivity can also be fitted with a function $k \propto T^{-n}$ for comparison to the theoretical thermal conductivity at high temperature. In the temperature range 30–50 K, the experimental curve, the fixed lattice parameter case, and the temperature-dependent lattice parameter case have values of the exponent n equal to 1.22, 1.16, and 1.10, respectively. These values are all in reasonable agreement and are slightly larger than the high temperature thermal conductivity exponent $n = 1$. In the temperature range 50–70 K, the values are 1.4, 0.617, and 1.55, respectively. Here the exponent for the fixed lattice parameter case deviates dramatically from that for the experimental and the temperature-dependent lattice parameter cases, and the exponents for the experimental and temperature-dependent cases increase further. These phenomena indicate that thermal expansion effects should not be neglected at high temperatures in solid argon.

Although the trend of thermal conductivity dependence

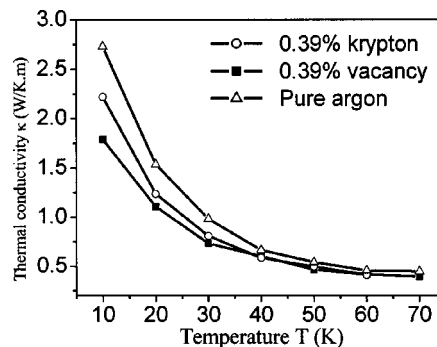


FIG. 3. Defect and impurity effects on thermal conductivity of solid argon.

on temperature for the temperature-dependent lattice parameter case in Fig. 2 is correct, the calculated data are lower than experimental data over the entire temperature range and are also lower than the fixed parameter case data. Since experimental samples typically have defects and impurities that scatter phonons, and since no impurities have been introduced into the simulation model, simulations should yield higher values than experiments. This discrepancy is attributed to the LJ potential itself. Although the temperature dependence of argon lattice constants is available, there is no such information on the temperature dependence of the energy parameter in the LJ potential. The only temperature for which these parameters are available is 0 K; the values of these parameters were found by Pollack^{22,23} and are shown in Table I. The procedure they used to obtain these parameters results in a weaker energy scale in the LJ potential than that existing in reality,²⁴ leading to weaker interactive forces among atoms and thus a lower thermal conductivity than the experimental results.

As described above, thermal expansion leads to a deviation of the temperature dependence in thermal conductivity from $k \propto T^{-1}$. Another interesting problem is to determine the effect of the impurity and defect scattering processes on the thermal resistance at higher temperatures. In the present simulations, both impurities and vacancy defects in solid argon are investigated for a 516-atom system. This is accomplished by replacing one argon atom with a krypton atom or a vacancy, which gives us a defect concentration of 0.39%.

Figure 3 shows the impurity and vacancy effects on the thermal conductivity. The simulation results indicate that defects decrease the sample thermal conductivity and that the temperature dependence of thermal conductivity becomes less pronounced as temperature increases. The results also show that for the same defect density, the thermal conductivity with a vacancy defect is smaller than that with a krypton impurity. According to Eq. (15), the reciprocal of impurity scattering time is proportional to the square of the difference in mass between a defect and the surrounding material. Table I indicates that the mass difference between a vacancy defect and the argon lattice is smaller than that for a krypton defect in an argon lattice. The inverse relaxation time scale τ_i^{-1} of a vacancy scattering is thus smaller than that for a krypton impurity scattering, leading to a prediction by Eq. (5) of larger conductivity for the lattice with the va-

cancy defect. This theoretical result contradicts the current EMD results.

The insertion of a defect displaces the surrounding atoms and induces strain in the lattice. The velocity of the phonons is changed by the variation in interatomic distance, leading to a change in direction and a phonon scattering event. Such strain effects are neglected in Eq. (15), which only considers the mass difference contribution to impurity scattering. The relaxation time due to the relative displacement of the neighboring atoms is given by¹²

$$\tau_s^{-1} = A_s \omega^4, \quad (17)$$

where

$$A_s = \frac{2V_0}{\pi^2 v_s^3} Q_0^2 \gamma^2 \sum_{i=1}^n f_i \left(1 - \frac{R_i}{R}\right)^2, \quad (18)$$

where R_i and R indicate the radii of the impurity and host atoms and γ indicates the Grüneisen parameter. Typical values of the parameter Q_0 reported for K^+ impurities in NaCl and vacancies in KCl are listed in Table I. Adding strain effects [Eq. (17)] to the mass difference term [Eq. (15)] leads to the following relation for point defect scattering:

$$\tau_p^{-1} = \tau_i^{-1} + \tau_s^{-1} = (A_i + A_s) \omega^4. \quad (19)$$

The values of A_i and A_s calculated from Eqs. (16) and (18) for vacancies and krypton impurities are listed in Table I. For both vacancies and krypton impurities, the strain coefficient A_s is about three orders larger than the mass difference coefficient A_i . Since the value of A_s is larger for a vacancy than for a krypton atom, the total inverse scattering time for krypton impurities is smaller than that for vacancies. The inclusion of lattice strain effects thus results in a lower thermal conductivity for vacancies than for krypton and removes discrepancies between the Callaway model and EMD simulations.

To analyze the defect scattering time further, EMD simulations were performed at a vacancy concentration density of 1.5%. The simulation data for these simulations as well as for simulations at 0.39% vacancy density and 0% vacancy density (pure argon) were fitted in the range 30–60 K as described in Sec. II, using the parameter $A = A_i + A_s$ as the only fitting parameter. The fitted values of A are 4.0E-38 for pure argon, 6.0E-38 for the 0.39% case, and 9.5E-38 for the 1.5% case. The Callaway model, adjusted to include strain effects, was used in conjunction with the above A values to calculate thermal conductivity. These theoretical calculations (curves) along with simulation results (points) are shown in Fig. 4. The parameter A can also be calculated directly from Eqs. (16) and (18). The directly calculated data are 2.84E-38 and 10.8E-38 for samples with vacancy densities 0.39% and 1.5%, respectively. The values of A from the fitting procedure are of the same order of magnitude as the directly calculated values, and for the 1.5% case agree within 15%. These results indicate that fitting of molecular dynamics simulation results is a viable alternative to direct calculation, using Eqs. (16) and (18), for determination of the parameter A .

The temperature dependence of theoretical thermal conductivity is also fitted with exponential functions for the pure

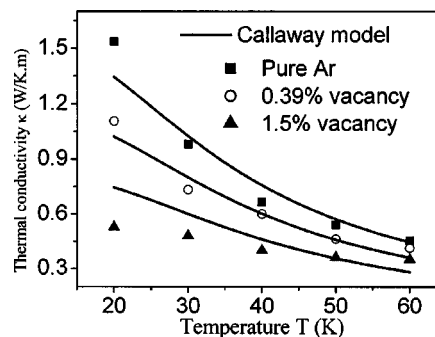


FIG. 4. Defect concentration effects on thermal conductivity of solid argon.

argon, 0.39%, and 1.5% cases. The values of n equal 1.14, 0.91, and 0.398 over the temperature range 30–60 K for the three theoretical curves, respectively. It is further confirmed that the temperature dependence in the thermal conductivity deviates greatly from $k \propto T^{-1}$ due to lattice strain resulting from the vacancy defects.

Figure 5 presents the effects of impurity concentration on the thermal conductivity at different temperature. The two curves represent simulations run at 30 and 50 K. With increasing temperature, the impurity effects on the lattice thermal conductivity are observed to diminish.

IV. CONCLUSION

Equilibrium molecular dynamics simulation is used to investigate thermal expansion and impurity effects on the lattice thermal conductivity of solid argon. The simulated thermal conductivity is not sensitive to the simulated cell size. Over the temperature range 20–80 K, the simulated results agree well with the experimental results. However, the thermal conductivity deviates greatly from the measured data below 20 K, which implies that the classical molecular dynamics simulation method is not appropriate far below the Debye temperature. The simulation results prove that thermal expansion contributes to thermal resistance, particularly at high temperatures. This article reports that the coefficients of the relaxation time scale due to impurity scattering can be quantitatively fitted from molecular dynamics. The calculations show an order of magnitude agreement with the data calculated directly from theoretical models, and for the case of 1.5% vacancy defect density the agreement falls within 15%. Based on the simulated thermal conductivity for

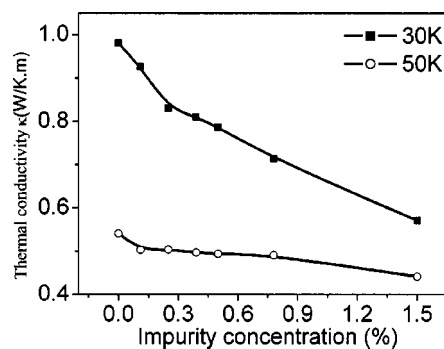


FIG. 5. Thermal conductivity of solid argon at different temperatures.

samples with vacancy defects and impurity atoms of krypton, it is found that phonon scattering on impurities due to lattice strain is much stronger than that due to mass difference. Argon with vacancy defects is thus found to have a lower thermal conductivity than argon with krypton impurities at the same defect concentration.

ACKNOWLEDGMENTS

One of the authors (Y.C.) acknowledges the financial support of the China Natural Science Foundation (50276011, 50275026) and the 863 High Technology Program (Project No. 2003 AA404160).

¹J. M. Ziman, *Electrons and Phonons* (Clarendon, Oxford, 1960).

²I. N. Krupskii and V. G. Manzhelli, *Phys. Status Solidi* **24**, K53 (1967).

³F. Clayton and D. N. Batchelder, *J. Phys. C* **6**, 1213 (1973).

⁴J. S. Dugdale and D. K. MacDonald, *Phys. Rev.* **98**, 1751 (1955).

⁵D. K. Christen and G. L. Pollack, *Phys. Rev. B* **12**, 3380 (1975).

⁶J. Callaway, *Phys. Rev.* **113**, 1046 (1959).

⁷Y. C. Tai, C. H. Mastrangelo, and R. S. Muller, *J. Appl. Phys.* **65**, 1442 (1988).

⁸W. S. Capinski, H. J. Maris, E. Bauser, I. Silier, M. Asen-Palmer, T. Ruf, M. Cardona, and E. Gmelin, *Appl. Phys. Lett.* **71**, 2109 (1997).

⁹M. Asen-Palmer, K. Bartkowski, E. Gmelin, M. Cardona, A. P. Zhernov,

A. V. Inyushkin, A. Taldenkov, and V. I. Ozhogin, *Phys. Rev. B* **56**, 9431 (1997).

¹⁰P. G. Klemens, *Proc. R. Soc. London, Ser. A* **208**, 108 (1951).

¹¹G. V. Paolini, P. J. D. Linda, and J. H. Harding, *J. Chem. Phys.* **106**, 3681 (1997).

¹²M. Asheghi, K. Kurabayashi, R. Kasavi, and K. E. Goodson, *J. Appl. Phys.* **91**, 5079 (2002).

¹³P. Stachowiak, V. V. Sumarokov, J. Mucha, and A. Jez Bowski, *Phys. Rev. B* **58**, 2380 (1998).

¹⁴V. G. Plekhanov, *Mater. Sci. Eng., R.* **35**, 139 (2001).

¹⁵H. Kaburaki, J. Li, and S. Yip, *Mater. Res. Soc. Symp. Proc.* **538**, 503 (1998).

¹⁶S. G. Volz, J. B. Saulnier, M. Lallemand, B. Perrin, P. Depondt, and Mareschal, *Phys. Rev. B* **54**, 340 (1996).

¹⁷J. R. Lukes, D. Y. Li, X. G. Liang, and C. L. Tien, *J. Heat Transfer* **116**, 536 (2000).

¹⁸L. J. Porter, L. Ju, and S. D. Yip, *J. Nucl. Mater.* **246**, 53 (1997).

¹⁹B. K. Agrawal and G. S. Verma, *Phys. Rev.* **126**, 24 (1962).

²⁰O. G. Peterson, D. N. Batchelder, and R. O. Simmons, *Phys. Rev.* **150**, 703 (1966).

²¹P. K. Schelling, S. R. Phillpot, and P. Keblinski, *Phys. Rev. B* **65**, 144306 (2002).

²²G. A. Pollack, *Rev. Mod. Phys.* **36**, 748 (1964).

²³J. Corner, *Trans. Faraday Soc.* **44**, 914 (1948).

²⁴E. A. Guggenheim and M. L. McGlashan, *Proc. R. Soc. London, Ser. A* **255**, 456 (1960).